Polymer Bulletin
https://doi.org/10.1007/s00289-022-04667-4

ORIGINAL PAPER

# In-vitro release studies of ciprofloxacin drug using polyaniline/polypyrrole-encapsulated β-cyclodextrin nanocomposites

**Jannatun Zia[2] · Mohd Riyazuddin[2] · Shaila Jackson[1] · Darlene K. Taylor[1] · Ufana Riaz[1,2]**

Received: 17 August 2022 / Revised: 9 December 2022 / Accepted: 28 December 2022


## Abstract

The present study reports the synthesis of nanocomposites of β-cyclodextrin (β-CD) with polyaniline (PANI) and polypyrrole (PPy) to design core–shell nanocomposites. The synthesized nanocomposites were investigated for their spectral, morphological and thermal characteristics. IR spectra confirmed the incorporation of PANI and PPy in β-CD by the strong interaction between NH of PANI/PPY and OH of β-CD, while the ultraviolet (UV)-visible spectra confirmed the polaronic state of conducting polymers in the nanocomposites. The scanning electron microscopy (SEM) analysis revealed the core–shell like morphology of the nanocomposites. Ciprofloxacin (CIP) was chosen as a model drug to study the in-vitro drug release as gastric (pH 1.2) and intestinal (pH 7.4) values by loading the drug (50 mg) into the pristine polymers as well as β-CD nanocomposites. The nanocomposites were found to show the sustained release behavior and hold potential to be used as an effective antibiotic drug delivery vehicle.

**Keywords** Polyaniline · Polypyrrole · β-cyclodextrin · Ciprofloxacin · Adsorption · Drug release kinetics

✉ Ufana Riaz
ufana2002@yahoo.co.in; uriaz@nccu.edu

[1] Department of Chemistry and Biochemistry, North Carolina Central University, Durham, NC 27707, USA

[2] Department of Chemistry, Materials Research Laboratory, Jamia Millia Islamia, New Delhi 110025, India

Published online: 02 January 2023

## Introduction

Current research is focused toward the designing of drug delivery vehicles that can facilitate site specific controlled release, reduce side effects and also balance the drug concentration in an optimal range in the human body [1–3]. For the past few decades, conducting polymers (CPs) have been extensively investigated for their spectral, morphological and thermal properties which could be utilized in a variety of applications [4–12]. They also serve as ideal candidates for designing drug delivery systems due to their electro-active nature which helps in binding of various kinds of drugs [13–17]. CPs such as polypyrrole (PPy) [18], polyaniline (PANI) [19], polythiophene (PTh) [20], poly(o-phenylenediamine) (POPD) [21], polycarbazole (PCz) [22], and poly(1-naphthylamine) (PNA) [23, 24] have been used in the design of the drug delivery systems. Literature survey reveals that the PPy and PANI have shown controlled release behavior when used as a drug delivery vehicle [25–32]. Interestingly, these polymers also exhibit remarkable host–guest relationships due to their ease of diffusion in the cavities of various kinds of molecules [16, 21, 22, 33].

Cyclodextrins (CDs) are cyclic oligosaccharides that consist of glucose monomer units and show the capacity to incorporate guest molecules in their cavities which can from inclusion complexes with a variety of organic compounds and have been extensively used as drug delivery systems [34–39]. β-CD as the modifying agent with a hydrophilic exterior and a hydrophobic interior forms inclusion complexes with polymers [40]. Modification of the properties of β-CD molecules with conducting polymers is a facile technique that can be adopted to design drug delivery vehicles which can increase the solubility of poorly soluble drugs, stabilize the drugs and also control the their release characteristics [12, 41–45].

Although a lot of works have been reported on the β-CD, till date no study has been reported on the use of ultrasound-assisted polymerization of conducting polymer with β-CD for their application as drug delivery vehicles. In the present research work, we have synthesized PANI and PPy nanocomposites via ultrasound-assisted in-situ polymerization of the monomers in the β-CD solution. The synthesized nanocomposites were characterized using FTIR, UV–visible, X-ray diffraction (XRD), scanning electron microscopy (SEM) and thermogravimetric analysis (TGA) techniques. Ciprofloxacin (CIP) was selected as the model drug which is used most commonly as antibiotic drug in various kinds of treatment. The release behavior of CIP drug was investigated using pristine PPy, PANI, PPy/β-CD and PANI/β-CD nanocomposites at gastric and intestinal pH values for a period of 3 h. Kinetic models such as pseudo-first-order, pseudo-second-order, Elovich and intra-particle diffusion were used to investigate the adsorption mechanism, while the release kinetics was explored using zero-order, first-order, Higuchi and Korsmeyer–Peppas models.

## Materials

Pyrrole ($C_4H_5N$) (molar mass: 67.09 g/mol, density: 0.967 g/cm$^3$, melting point: − 23 °C, boiling point: 129–131 °C) and aniline ($C_6H_5NH_2$) (molar mass: 93.13 g/mol, density: 1.02 g/cm$^3$, melting point: 6.3 °C, boiling point: 184.1 °C) were procured from Sigma-Aldrich, USA. Ferric chloride ($FeCl_3$) (molar mass: 162.20 g/mol), ethanol ($C_2H_5OH$) (molar mass: 46.07 g/mol, density: 0.7893 g/cm$^3$, melting point: − 114.14 ± 0.03 °C, boiling point: 78.24 ± 0.09 °C), and hydrochloric acid (35% HCl) (molar mass: 36.46 g/mol, density: 1.16 g/cm$^3$) were procured from Merck, India. Ammonium persulfate ($(NH_4)_2S_2O_4$) (molar mass: 228.19 g/mol)) was procured from HPLC laboratory, India. β-cyclodextrin (molar mass: 1134 g/mol) was procured from Loba Chemie, India, and Ciprofloxacin ($C_{17}H_{18}FN_3O_3$) (molar mass: 331.346) was procured from Cipla, India.

### Synthesis of polypyrrole (PPy)

1.3 ml (0.02 mol) of pyrrole monomer was dispersed in distilled water (30 ml) in 100-ml conical flask and solution was sonicated for 30 min at a temperature at 25 °C. $FeCl_3$ (3.24 g, 0.02 mol) was dissolved in 30 ml of distilled water and added dropwise into the pyrrole dispersion during sonication. The reaction mixture was then further sonicated for 4 h at 25 °C. The synthesized dark black color precipitate of PPy was centrifuged, washed several times with distilled water and dried in vacuum oven at 60 °C for 24 h.

### Synthesis of polyaniline (PANI)

Aniline (1.8 ml, 0.02 mol) was dispersed in 35% HCl (0.2 M, 30 ml) in a 100-ml conical flask and the dispersion was sonicated for 30 min at 0 °C. Ammonium persulfate (4.5 g, 0.02 mol) was dissolved in 30 ml of 35% HCl solution (0.2 M) and added into another 100 ml conical flask. After 30 min, the APS solution was mixed with the aniline dispersion and further sonicated for 4 h at 25 °C. The dark bluish-green color precipitate of PANI was then centrifuged and washed several times with distilled water, ethanol, dried in vacuum for 24 h at 80 °C to ensure the complete removal of water.

### Preparation of β-CD/PPY and β-CD/PANI nanocomposites

β-CD (2.269 g, 0.002 mol) was added in a 150-ml conical flask containing distilled water (50 ml) and stirred on a magnetic stirrer for 30 min. Pyrrole monomer (0.277 ml) was added to the β-CD solution and stirred vigorously for another 30 min. Ferric chloride (0.650 g, 0.004 mol) was dissolved in 50 ml distilled water to prepare the oxidant solution. The ferric chloride solution was then transferred to the β-CD solution. During the mixing process, the solution color changed to dark green, indicating polymerization of the monomer. The polymerization was carried out for 24 h at 25 °C. The resulted black precipitate was filtered and washed with the

sufficient amount of distilled water and dried in a vacuum 70 °C for 48 h. **S**imilar method was adopted for other monomer (aniline), and the nanocomposites were designated as β–CD/PPy and β-CD/PANI respectively.

### Loading of ciprofloxacin (CIP) drug in PPy, PANI, β-CD, β-CD/PPy and β-CD/PANI nanocomposites

PPy (100 mg) powder was homogeneously mixed with ciprofloxacin (50 mg) using a mortar pestle. The mixture was then dispersed in deionized water (30 ml) and stirred on the magnetic stirrer for a period of 2 h at 40 °C. The drug loaded solution was centrifuged and dried in vacuum oven at 60 °C. Similar method was adopted for loading CPFX in PANI, β-CD/PPy and β-CD/PANI nanocomposites. Drug-loaded samples were designed as PANI-CPFX-50, PPy-CPFX-50, β-CD/PPy-CPFX-50 and β-CD/PANI-CPFX-50, respectively. The amount of equilibrium (Qe), drug adsorption (β), percentage of loading and encapsulation efficiency of drug were calculated by equations reported by *Verma* et al. [13–16, 33]. The experiments were carried out in triplicate.

### Preparation of dissolution medium and adsorption and in-vitro drug release studies of PPy, PANI, β-CD/PPy and β-CD/PANI nanocomposites.

The intestinal fluid medium (pH = 1.2 and pH = 7.4) was prepared by method reported in our earlier studies [13–16, 33]. Dissolution experiment was carried out using dissolution tester model (DS 1400 LABINDIA, India). Dialysis bag was dipped in to the receptor compartment containing 500 mL of prepared dissolution medium (buffer solution) and stirring at 37.5 °C. The dissolution medium (5 mL) was withdrawn at 30-min time interval, and the same volume was replaced with a fresh dissolution medium. Samples were analyzed for release of CIP spectroscopically at $\lambda_{max} = 330$ nm. Amount of drug release, concentration of drug, and cumulative drug release were calculated by equation as per reported method by *Verma* et al. [13, 14, 33]. The drug release kinetics, Elovich and parabolic diffusion models were employed as per details given in our previous studies [16, 33]. The experiments were carried out in triplicate.

## Characterization

### Spectral analysis

IR spectra of pure PPY, PANI, β-CD, β-CD/PPY and β-CD/PANI nanocomposites were recorded in powder form on Shimadzu Model IRA Affinity. UV–Visible spectra of PPy, PANI, β-CD, β-CD/PPy and β-CD/PANI nanocomposites were taken on UV–visible spectrophotometer Model Shimadzu UV-1800.

### Morphological analysis

X-ray diffraction patterns were recorded using Rigaku Ultima IV X-Ray diffractrometer using Ni filtered Cu-Kα radiation. All measurements were carried out in powder form and d-spacing were calculated using Braggs equation. Scanning electron microscopy (SEM) images were obtained using FE-SEM model EVO18, Carl Zeiss, Germany,

### Thermal analysis

The thermal stability of synthesized PPy, PANI, β-CD/PPy and β-CD/PANI nanocomposites was investigated using thermal analyzer on thermal analyzer STA6000, Exstar as per the previously reported method [30]. The samples were heated from 35 to 600 °C at the rate of 10 °C $min^{-1}$ in $N_2$ atmosphere.

## Results and discussion

### Confirmation of loading of conducting polymers in β-CD/PPy and β-CD/PANI nanocomposites

The TGA profile of pristine β–CD (Fig. 1) showed observed 10 wt.% loss at 150 °C due to moisture, while 50 wt.% loss occurred at 320 °C. Almost complete degradation took place at 600 °C. Pristine PPy revealed hardly 10 wt.% degradation at 220 °C, while almost 30% degradation took place at 355 °C and almost 45 wt.% degradation was noticed at 600 °C, Similarly, the TGA profile of pristine PANI showed 10 wt.% degradation around 200 °C, while 30 wt.% degradation took place at 310 °C

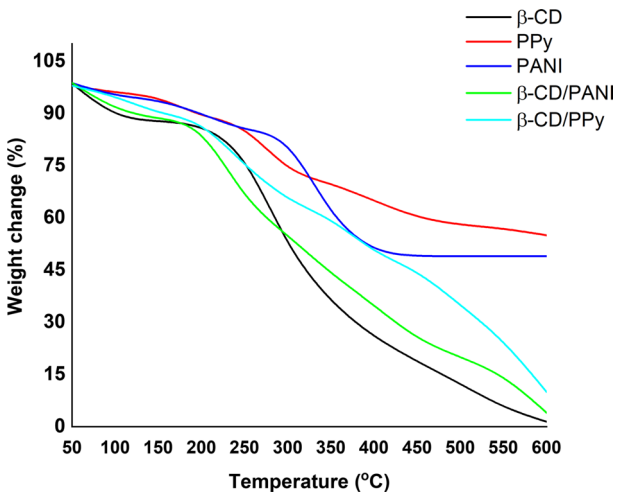


**Fig. 1** TGA thermogram of PPy, PANI, β-CD/PPy and β-CD/PANI nanocomposites

and almost 51 wt.% degradation took place at 600 °C. The nanocomposites of PANI and PPy with β-CD showed lower stability as compared to pristine polymers due to higher loading of β-CD as compared to the conducting polymers in the nanocomposites. The TGA profile of β-CD exhibited the first thermal degradation event at 150 °C exhibiting 10 wt.% loss at this temperature and 33 wt.% loss was noticed at 315 °C, while at 600 °C almost 90 wt.% loss was noticed. Hence, based on the weight loss of pristine PPy at 600 °C and that of β-CD/PPy, the loading of PPy in this nanocomposite was computed to be 45% as per method reported in our previous studies [9, 11, 12]. Similarly, for the β-CD/PANI nanocomposite, the first decomposition event was observed at 200 °C showing 12 wt.% loss, while almost 55 wt.% loss occurred at 300 °C. Almost 96 wt.% loss was noticed at 600 °C. The loading of PANI in this nanocomposite was computed to be almost 45%. The thermal stability was found to follow the order β-CD < β-CD/PANI < β-CD/PPy < PANI < PPy.

## IR analysis and confirmation of nanocomposite formation

The IR spectra of synthesized PPY, PANI, β-CD/PPy and β-CD/PANI nanocomposites are depicted in Fig. 2a, b. IR spectra for β-CD have been reported by other authors which was found to show peaks at 3134 $cm^{-1}$, 1612 $cm^{-1}$,1403 $cm^{-1}$ 1157 $cm^{-1}$, 1078 $cm^{-1}$, 1028 $cm^{-1}$, and 1001 $cm^{-1}$ which corresponded to stretching vibrations of $(OH)_{\nu}$, $(C–C)_{\nu}$ and bending vibration of $(O–H)_{\nu}$ respectively [16]. The IR spectrum of pure PPy (Fig. 2a) showed NH stretching vibration peak at 3417 $cm^{-1}$ and 3051 $cm^{-1}$, while the peak at 1683 $cm^{-1}$ confirmed C=C stretching [4, 10]. The typical peaks observed at 1599 $cm^{-1}$, 1447 $cm^{-1}$ and 1325 $cm^{-1}$ were as ascribed to the pyrrole ring C–H stretching. The peak at 1237 $cm^{-1}$ was associated with C–N stretching vibration. The peaks at 927 $cm^{-1}$, 842 $cm^{-1}$, 803 $cm^{-1}$,747 $cm^{-1}$ and 722 $cm^{-1}$ were associated with the deformation of the five-membered ring and C–H wagging.

The IR spectrum of β-CD/PPy (Fig. 2a) revealed a broad hump at 3265 $cm^{-1}$. Since this region is associated with the OH of β-CD and NH of PPy, it is evident that hydrogen bonding takes place between NH of PPy and OH of β-CD which was corroborated by the broadness in the peak intensity corresponding to the OH stretching vibration of pristine β-CD [16]. Moreover, the NH and OH peaks were not noticed to exist independently in this region which also confirmed the intense interaction between the two functional groups via hydrogen bonding. The peak at 2912 $cm^{-1}$ was noticed due to the C–H stretching vibrations of β-CD. The peaks at 1641 $cm^{-1}$ and 1531 $cm^{-1}$ were correlated to the pyrrole ring C=C stretching, C–H stretching vibration modes as noticed in the pristine spectrum of PPy. The OH bending vibration mode of β-CD appeared at 1151 $cm^{-1}$, while the peak at 1023 $cm^{-1}$ was associated with the OH bending mode of β-CD. The peaks at 856 $cm^{-1}$, 753 $cm^{-1}$ were associated with the C–H wagging of PPy. The spectrum showed co-existence of PPy and β-CD peaks and hydrogen bonding between NH of PPy and OH of β-CD which confirmed formation of nanocomposite. The IR spectrum of PANI (Fig. 2b) showed a sharp peak at 3414 $cm^{-1}$ and 3047 which were attributed to the N–H stretching vibrations, while the peaks at

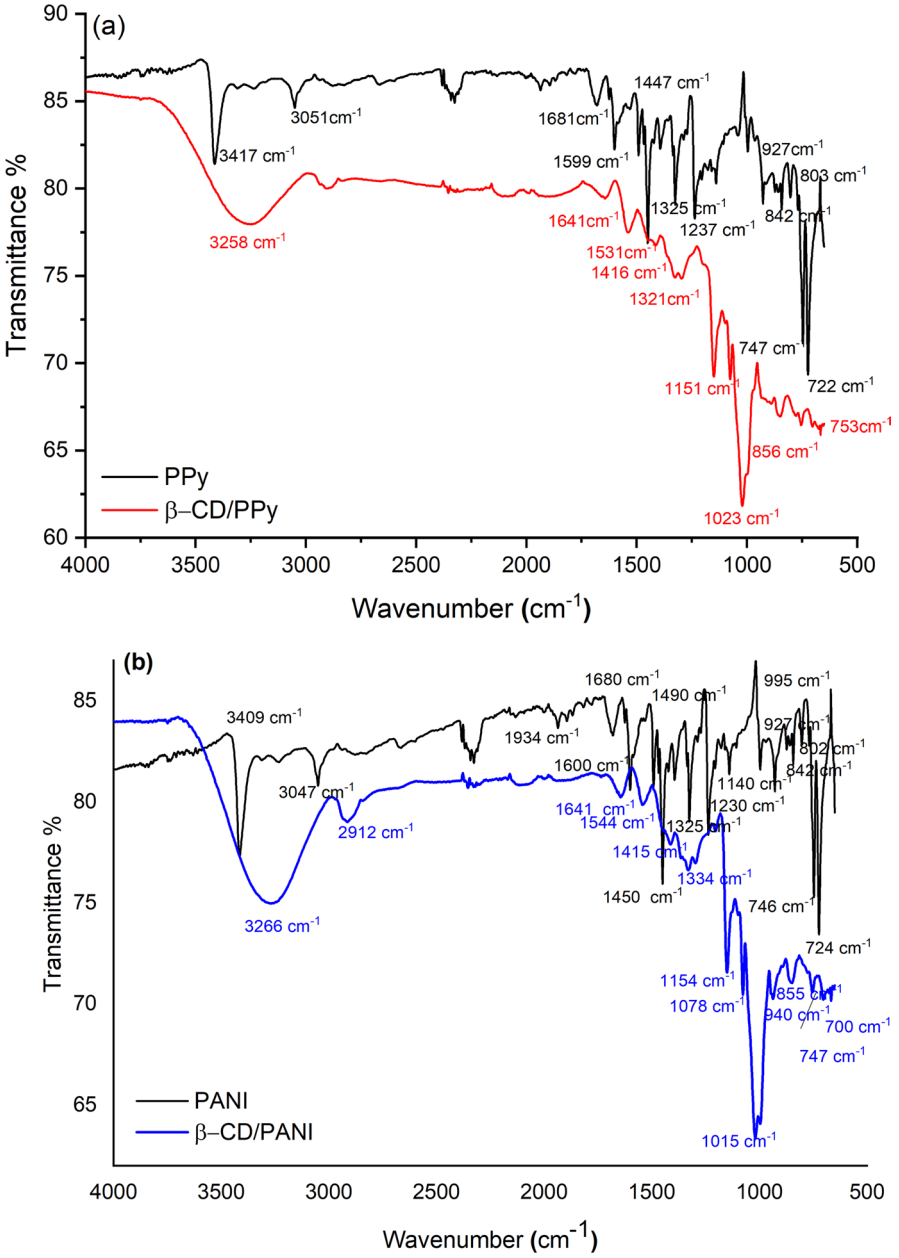


**Fig. 2** IR spectra of **a** PPy and β-CD/PPy, **b** PANI and β-CD/PANI nanocomposites

1680 $cm^{-1}$,1600 $cm^{-1}$, 1490 $cm^{-1}$ and 1325 $cm^{-1}$ were correlated to the imine and benzenoid stretching vibrations, respectively. The peak at 1230 $cm^{-1}$ was

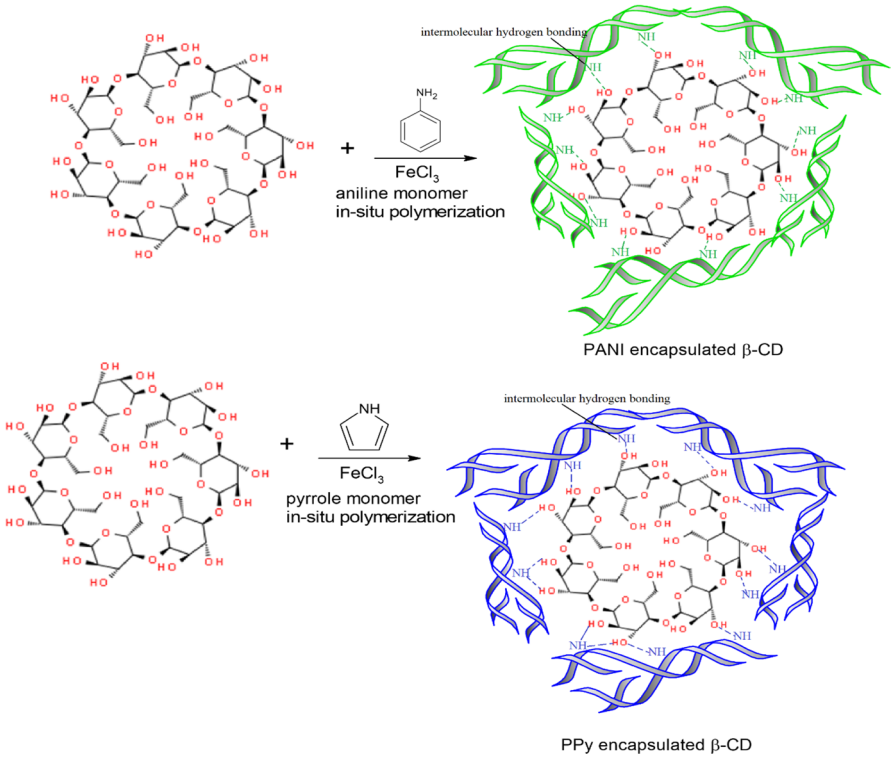


**Scheme 1** Mechanism of in-situ polymerization of PANI and PPY in presence of β-CD

assigned due to the CN stretching vibration. The peaks at 1140 $cm^{-1}$, 995 $cm^{-1}$ and 927 $cm^{-1}$ were associated with aromatic ring stretching and deformation modes. The IR spectrum of β-CD/PANI nanocomposites showed OH stretching vibration peak at 3266 $cm^{-1}$ and similar to the spectrum of β-CD/PPy; this region was an overlap region of OH of β-CD and NH of PANI. Since no separate peaks were observed for the two components but a hump was observed in this region, it was attributed to NH –OH bonding between PANI and β-CD. The peak at 2912 was correlated to the C–H stretching vibration of β-CD. The benzenoid and quinonoid peaks were noticed at 1544 $cm^{-1}$, 1415 $cm^{-1}$ and 1322 $cm^{-1}$. The peak at 1153 was attributed to the OH bending of vibration of β-CD. The peaks at 1078 $cm^{-1}$ 1015 $cm^{-1}$ were also associated with the bending of vibration of β-CD. The peaks at 940 $cm^{-1}$, 855 $cm^{-1}$, 747 $cm^{-1}$ and 700 $cm^{-1}$ were associated with the aromatic ring of PANI. The IR studies therefore confirmed the formation of β-CD/PANI nanocomposites as depicted in Scheme 1. Since the NH groups in the PANI and PPy chains bind with the OH of β-CD, we presume that the chains encapsulate the β-CD molecule and hence no major changes in the crystallinity of

β-CD should be seen. This observation is confirmed form the XRD studies in the proceeding section.

### XRD analysis of PPy, PANI, β-CD/PPy and β-CD/PANI nanocomposites

The XRD pattern of β-CD (Fig. 3) showed characteristic peaks at 2θ = 10.9°, 12.6°, 15.7°, 16.9°, 18.9°, 19.7°, 21.1°, 22.8°, 24.3°, 25.8°, 27.2°, 28.8°, 31.91°, and 34.70° associated with the presence of (041), (141), (180), (042), (162), (222), (223), and (044) planes (given as supplementary information as Figure S1). The XRD pattern of PPy (Fig. 3) revealed a broad hump at 2θ = 25.67° associated with the presence of (104) plane. The XRD profile of β –CD/PPy exhibited peaks at 2θ = 10.6°, 12.5°, 15.32°, 17.1°, 17.7°, 18.87°, 19.51°, 21.4°, 2.6°, 24.3°, 26.5°, 27.12°, 28.65°, 30.17° and 34.74° which were corresponded to the (011), (130), (014), (141), (090), (112), (180), (230), (091), (042), (251), (162), (222), (223) and (004) planes, and these planes were identified to match with the XRD pattern of β-CD (given in supporting information as Figure S1), while the peak noticed at 25.70 was associated with presence of PPy. The XRD pattern of pristine PANI showed peaks at 2θ = 17.9°, 18.82°, 20.01°, 23.3°, 25.10°, 26.21°, 30°, 32.18°, 35° and 40.60°. The XRD pattern of β –CD/PANI nanocomposites revealed peaks at 2θ = 10.6°, 12.5°, 15.32°, 17.1°, 17.7°, 18.87°, 19.51°, 21.4°, 22.6°, 24.3°, 26.5°, 27.12°, 28.65°, 30.17° correlated to

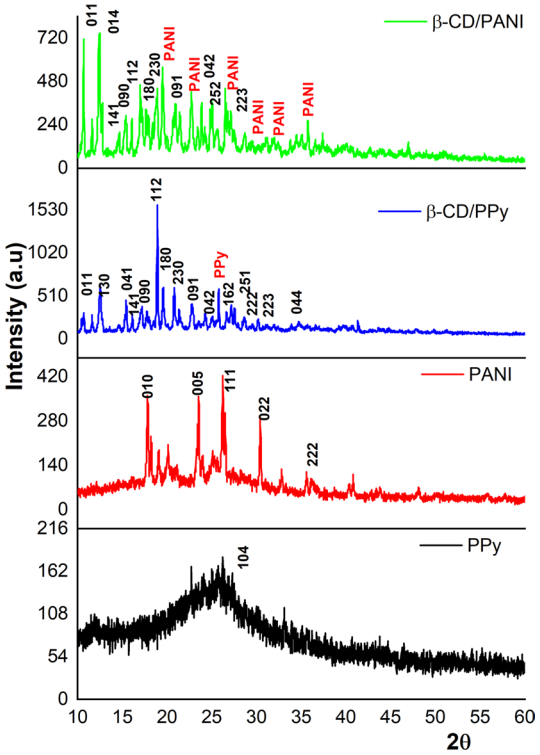


**Fig. 3** XRD profiles of PPy, PANI, β-CD/PPy and β-CD/PANI nanocomposites

XRD pattern of β-CD, while the peaks at 2θ = 20.01°, 23.3°, 25.10°, 26.21°, 32.18°, 35° and 40.60° were correlated to the presence of pure PANI. The results revealed that the XRD pattern of the nanocomposites exhibited a crystalline morphology which matched well with the XRD profile of pristine β-CD and the presence of planes associated with PPy and PANI in the XRD profiles confirmed the formation of a crystalline nanocomposite. It is interesting to note that the semicrystalline nature of PANI and amorphous nature of PPy was not predominant upon nanocomposite formation. This was attributed to the encapsulation of the β-CD structure by the conducting polymers which helped in keeping the crystallinity of the later intact. The XRD results also corroborated with the structure presented in Scheme 1.

## SEM analysis

The SEM of pristine PANI (Fig. 4a) showed the formation of entangled fibrous rods forming an intense network, while the SEM of PPy (Fig. 4b) showed the formation of spherical aggregates formed by joining tiny worm-like flexible rods. The morphologies were noticed to be well-organized in both polymers. The SEM image of β-CD/PANI (Fig. 4c) exhibited a dense granular morphology in which the rod-like

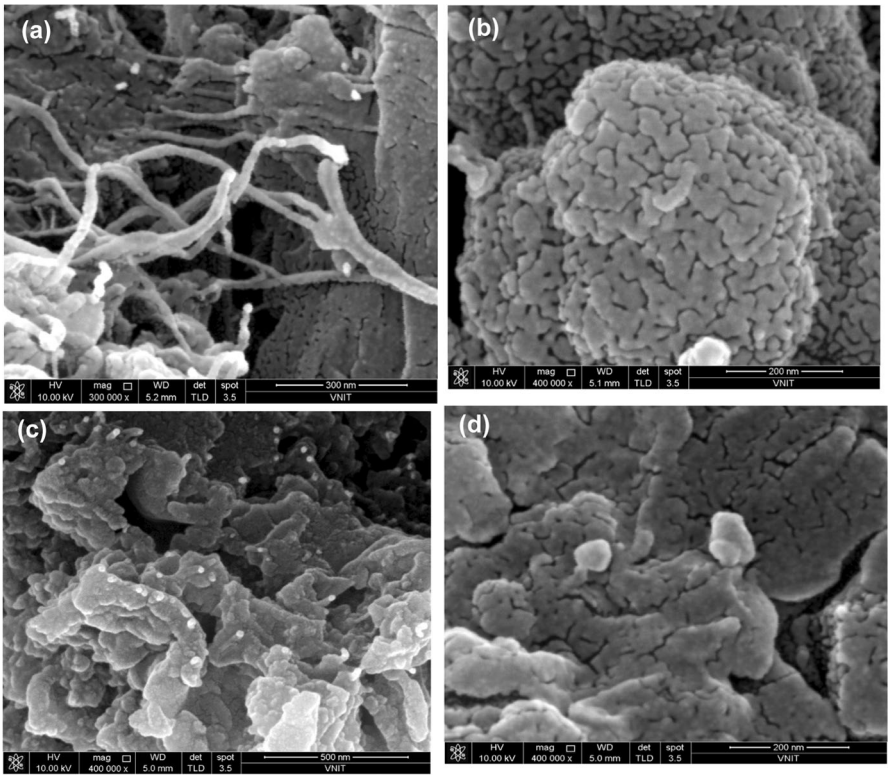


**Fig. 4** SEM images of **a** PANI, **b** PPy **c** β-CD/PANI, **d** β-CD/PPy

PANI structures seemed to be infused within the β-CD. The rod appeared to encapsulate the structure of β-CD by covering the entire surface. The structure revealed an aggregated morphology. The SEM of β-CD/PPy (Fig. 4d) revealed a morphology similar to the one observed for pure PPy suggesting that the surface was predominantly covered by PPy particles. However, the spherical aggregates were highly distorted in this case and formed a sheet-like structure. In this case also the PPy worm like rods appeared to be infused into a sheet-like layer. The morphologies of the nanocomposites revealed a predominance of the surface morphologies of PANI as well as PPy which further corroborates the encapsulation hypothesis.

### Variation in the electronic transitions of PPy and PANI upon nanocomposite formation with β-CD

The UV/Vis spectra were recorded to further confirm the changes in the electronic transition of PPy and PANI upon the formation of nanocomposites. The UV–vis spectrum of PPy (Fig. 5a) showed peaks at 250 nm, and 400 nm. The peak at 250 nm was associated with the π-π* transition, while the one around 400 nm was due to the polaronic transitions in PPy. The nanocomposite β-CD/PPy also revealed peaks at 265 nm and 400 nm but of lower intensity which was correlated to the electrostatic interaction between OH of β-CD and NH of PPy that causes lowering of the electronic transitions a β-CD is non-conducting and doesn't facilitate the charge transfer in PPy. Similarly, the UV–vis spectrum of PANI (Fig. 5b) exhibited peaks at 250 nm and 500 nm associated with the π-π* transitions and polaronic transitions in PANI and the nanocomposite showed the same transition at 245 and 500 nm. The suppression of the peak intensities of PANI upon nanocomposite formation was correlated to intense electrostatic interaction of the NH of the polymer with the OH group present in β-CD via intermolecular hydrogen bonding was responsible for the decrease in the electronic transition intensity of PANI. These results strongly suggest the encapsulation of the β-CD by PPy/PANI chains. The electrostatic interactions hinder charge transfer in PANI/PPy chains and lowers the absorption intensity. The shifting of the peaks is also caused by the electrostatic interaction between NH of PANI/PPy and OH of β-CD. Since the polymers have an intense interaction with the OH groups, this also prevents insertion of polymeric chains into the cage structure of β-CD leading to attachment of the polymers over the surface of the β-CD as shown in Scheme 1.

### Drug loading capacity, adsorption capacity and encapsulation efficiency of nanocomposites

The loading of CPFX (50 mg) was carried out as mentioned in "Preparation of dissolution medium and adsorption and in-vitro drug release studies of PPy, PANI, β-CD/PPy and β-CD/PANI nanocomposites". The loading of the drug in pristine conducting polymers showed that PANI revealed a slightly higher adsorption capacity in acidic as well as basic media as compared to PPy. The loading of the drug was higher in acidic media than in basic media due to

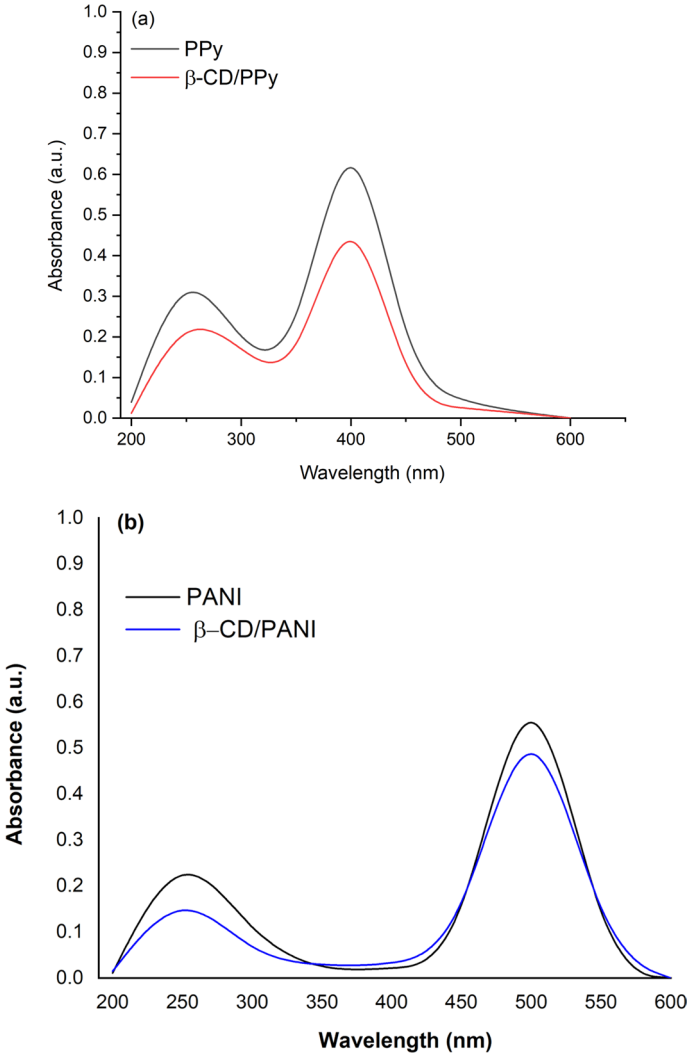


**Fig. 5** UV–visible spectra of **a** PPy and β-CD/PPy **b** PANI and β-CD/PANI

increase in the solubility of CPFX at low pH. Similarly, β-CD/PPy-CPFX-50 nanocomposite revealed lower adsorption capacity (7.34% ± 0.5) than β-CD/PANI-CPFX-50 (7.82 ± 0.5) containing same amount of the drug at pH 1.2 (Table 1). The nanocomposites have higher adsorption capacities than the pristine components. The encapsulation efficiency was noticed to be around 98% in acidic media as compared to basic media due to higher solubility of the drug in acidic media.

**Table 1** Adsorption capacity, encapsulation efficiency and percent loading of CPFX drug in nanocomposites at pH 1.2 and 7.4

| Sample | Amount of sample (Qe) (mg) | Adsorption capacity (%) ($\beta$) pH 1.2 | Adsorption capacity (%) ($\beta$) pH 7.4 | Encapsulation efficiency (%) pH 1.2 | Encapsulation efficiency (%) pH 7.4 | Drug content (%) pH 1.2 | Drug content (%) pH 7.4 |
|---|---|---|---|---|---|---|---|
| PANI-CPFX-50 | 50 | $6.26 \pm 0.5$ | $4.72 \pm 0.3$ | 95.32 | 90.56 | 94.48 | 90.32 |
| PPy-CPFX-50 | 50 | $5.54 \pm 0.5$ | $4.36 \pm 0.3$ | 96.63 | 91.43 | 94.43 | 91.76 |
| β-CD/PPy-CPFX-50 | 50 | $7.34 \pm 0.5$ | $4.83 \pm 0.3$ | 98.43 | 93.53 | 98.23 | 93.78 |
| β-CD/PANI-CPFX-50 | 50 | $7.82 \pm 0.5$ | $5.23 \pm 0.3$ | 98.67 | 94.63 | 98.72 | 94.84 |

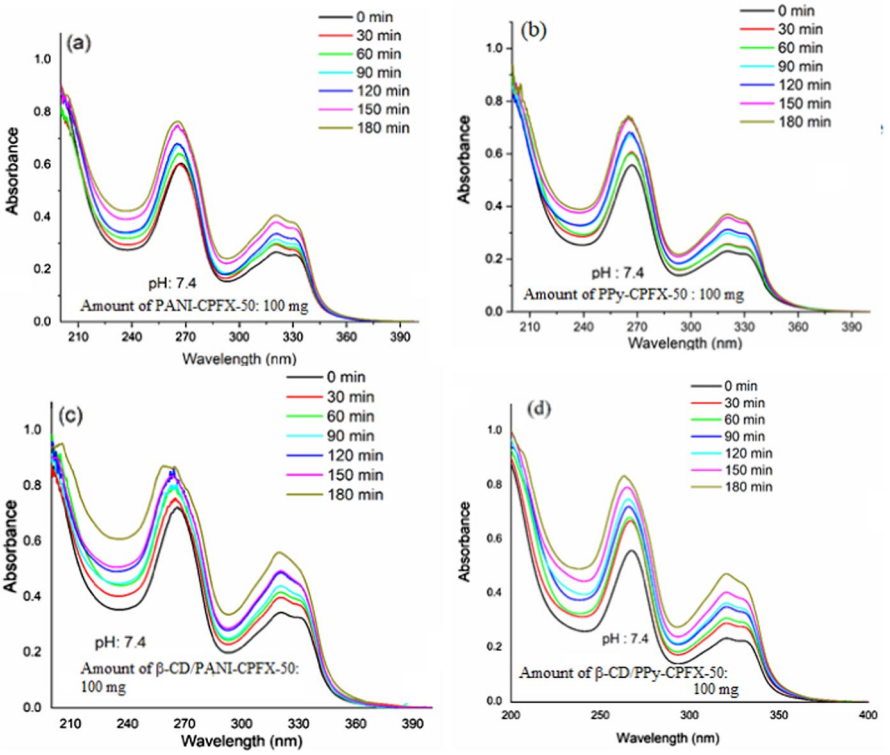


**Fig. 6** UV spectra of Ciprofloxacin (CPFX) drug release at pH 7.4 studied for a period of 180 min for **a** PANI-CPFX-50, **b** PPy-CPFX-50, **c** β-CD/PANI-CPFX-50 and **d** β-CD/PPy-CPFX-50 nanocomposites

## Release kinetics of ciprofloxacin drug from PPy-CPFX-50, PANI-CPFX-50, β-CD/PPy–CPFX-50 and β-CD/PANI-CPFX-50 nanohybrids

The drug release of CPFX was studied by UV analysis at two different pH and is depicted in Figs. 6, 7. The drug release at pH 7.4 and 1,2 was studied using PANI-CPFX-50, PPy-CPFX-50, β-CD/PANI-CPFX-50 and β-CD/PPy-CPFX-50 nanocomposites for a period of 180 min. CPFX drug revealed peaks at 275 nm and 325 nm which showed an increase in intensity with the increase in time (Fig. 6). The UV–visible spectrum of containing 100 mg of PANI-CPFX-50 (Fig. 7a) at pH 7.4 showed a noticeable increase in the absorbance intensity from 0.26 to 0.40 for the peak corresponding to 325 nm and from 0.59 to 0.75 for the peak corresponding to 275 nm. Similarly, while the UV–visible spectrum of PPy-CPFX-50 (Fig. 6b) showed increase in the 325 nm peak intensity 0.26–0.38 nm, the UV–visible spectrum of β-CD/PANI-CPFX-50 (Fig. 6c) revealed increase in the 325 nm peak intensity from 0.26 to 0.58, while β-CD/PPy-CPFX-50 (Fig. 6d) showed increase up to 0.56.

For the release studies in the acidic medium (Fig. 7a) pristine PANI-CPFX-50 exhibited increase in the peak intensity of the 325 nm peak of the CPFX drug

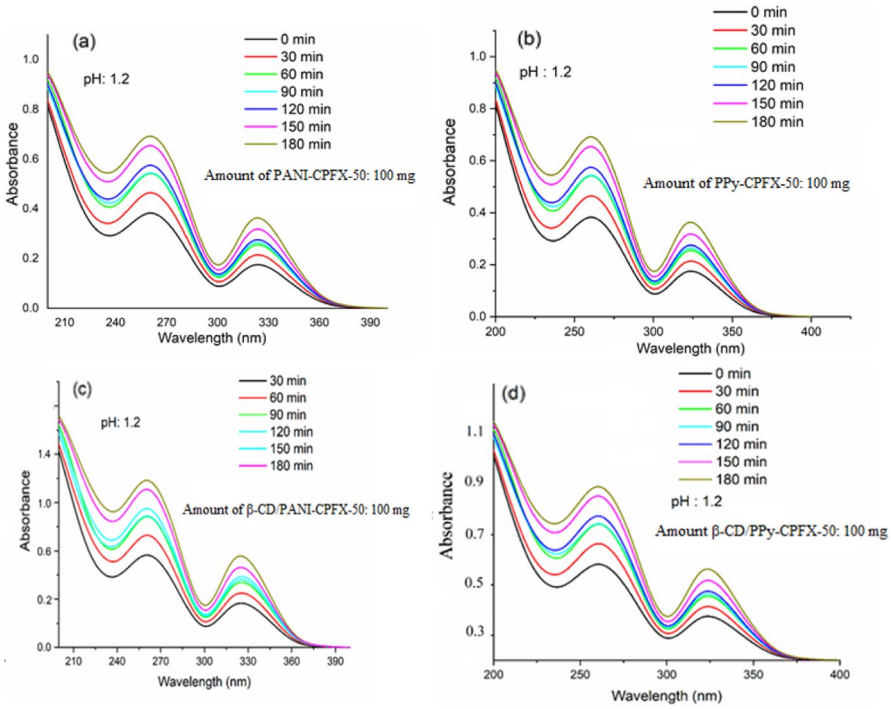


**Fig. 7** UV spectra of Ciprofloxacin (CPFX 50 mg) drug release at pH 1.2 studied for a period of 180 min for **a** PANI-CPFX-50, **b** PPy-CPFX-50, **c** β-CD/PANI-CPFX-50 and **d** β-CD/PPy-CPFX-50 nanocomposites

from 0.23 to 0.38, while pristine PPy-CPFX-50 (Fig. 7b) showed increase in the absorbance of the same peak from 0.23 to 0.37. The UV–vis spectrum of β-CD/PANI-CPFX-50 (Fig. 7c) showed increase in absorbance values from 0.23 to 0.62, while β-CD/PPy-CPFX-50 (Fig. 7d) showed increase up to 0.58. From the UV data, it can be concluded that β-CD/PANI-CPFX-50 showed highest release in acidic as well as basic media while among the pristine polymers, PANI-CPFX-50 showed higher release than PPy-CPFX-50.

The cumulative release studies showed that maximum release of almost 88% was attained in 180 min for β-CD/PANI-CPFX-50 in basic medium, while in acidic medium the release was 93% (Fig. 8a, b). The β-CD/PPPy-CPFX-50 nanocomposite showed 81% release in 180 min under basic medium, while 85% release was noticed in acidic medium (Fig. 8a, b). PANI-CPFX-50 and PPy-CPFX-50 showed 78% release and 741% release, respectively, in acidic medium (Fig. 8b), while the release was computed to be 68 and 60%, respectively, in basic medium (Fig. 8a). CPFX is ionized at low pH values and therefore becomes more soluble in acidic medium as compared to basic. β-CD contributes to an increase in solubility and therefore the nanocomposites reveal higher release as compared to pristine polymers.

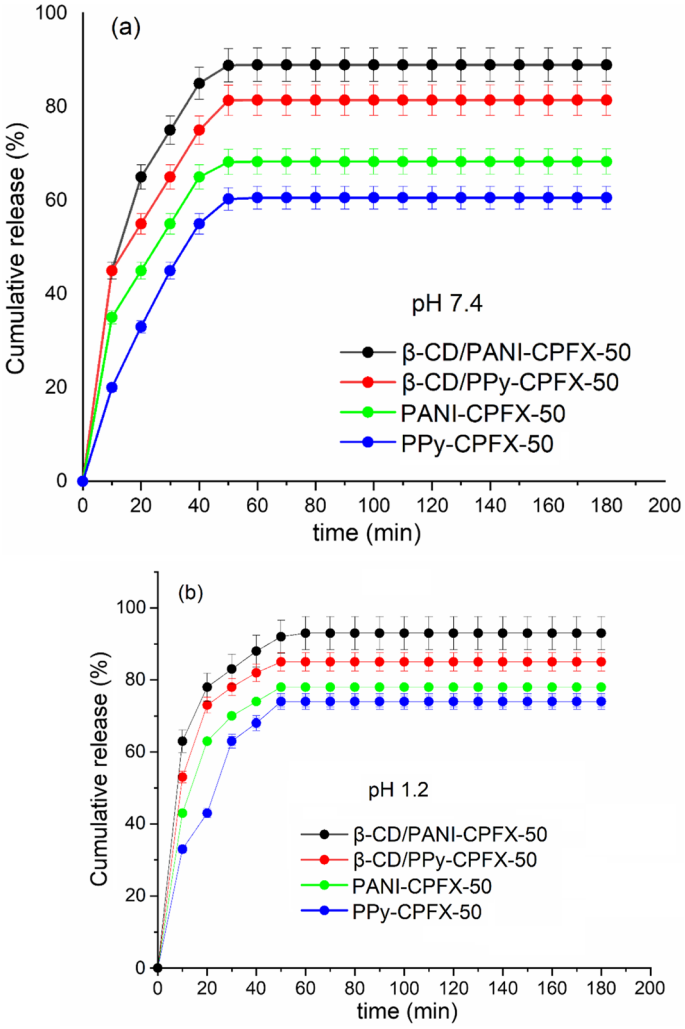


**Fig. 8** Cumulative release profiles for PANI-CPFX-50 PPy-CPFX-50, β-CD/PANI-CPFX-50 and β-CD/PPy-CPFX-50 nanocomposites

The pristine polymers as well as the nanocomposites followed the zero-order release kinetics in acidic as well as basic media as evident from the $R^2$ values which showed instant release of the drug followed by sluggish release. It was noticed that the rate constant values were observed to be highest for β-CD/PANI-CPFX-50 and lowest for PPy-CPFX-50 (Table 2). Pure PANI-CPFX-50 showed rate constant ($k$) value of $2.43\times10^{-1}$ at pH 7.4 for parabolic diffusion model, while the zero-order model exhibited $k$ value of $3.66\times10^{-1}$. The $k$ value was noticed to be one order higher for in acidic medium as compared to basic medium. The release kinetics also followed the parabolic diffusion model which confirmed that that the release process

**Table 2** Correlation coefficient values and drug release kinetics using zero-order kinetics parabolic diffusion model and Elovich model

| Sample | Zero-order kinetics | | Parabolic diffusion | | Elovich model | |
|---|---|---|---|---|---|---|
| | ($R^2$) | Rate constant | ($R^2$) | Rate constant | ($R^2$) | Rate constant |
| *(pH 7.4)* | | | | | | |
| PANI-CPFX -50 | 0.9807 | $3.66 \times 10^{-1}$ | 0.9987 | $2.43 \times 10^{-1}$ | 0.9106 | $1.34 \times 10^{-3}$ |
| PPy-CPFX-50 | 0.9819 | $3.54 \times 10^{-1}$ | 0.9980 | $2.32 \times 10^{-1}$ | 0.9226 | $1.25 \times 10^{-3}$ |
| β-CD/PPy-CPFX-50 | 0.9914 | $4.46\ 10^{-1}$ | 0.9930 | $3.19 \times 10^{-1}$ | 0.9394 | $1.36 \times 10^{-2}$ |
| β-CD/PANI-CPFX-50 | 0.9925 | $4.76\ 10^{-1}$ | 0.9964 | $3.72 \times 10^{-1}$ | 0.9497 | $1.38 \times 10^{-2}$ |
| *(pH 1.2)* | | | | | | |
| PANI-CPFX -50 | 0.9917 | $4.26 \times 10^{-1}$ | 0.9938 | $3.42 \times 10^{-1}$ | 0.9308 | $2.52 \times 10^{-3}$ |
| PPy-CPFX-50 | 0.9919 | $4.32 \times 10^{-1}$ | 0.9943 | $3.17 \times 10^{-1}$ | 0.9286 | $2.03 \times 10^{-3}$ |
| β-CD/PPy-CPFX-50 | 0.9924 | $4.46\ 10^{-1}$ | 0.9920 | $3.59 \times 10^{-1}$ | 0.9354 | $2.33 \times 10^{-2}$ |
| β-CD/PANI-CPFX-50 | 0.9932 | $4.66\ 10^{-1}$ | 0.9914 | $3.82 \times 10^{-1}$ | 0.9435 | $2.48 \times 10^{-2}$ |

of guest molecule (PANI/PPy-drug) by host (β-CD) was controlled by intra-particle diffusion/ surface diffusion process. The results suggested that for parabolic model, the release was diffusion-controlled processes/heterogeneous diffusion processes. The mechanism of drug release can be proposed on the basis that the initial fast release as seen from the cumulative release profiles is associated with unbounded CPFX molecules present on the surface. In acidic solution, the solubility of CPFX increases and therefore the electrostatic repulsions between the NH groups of PANI/PPy with the OH as well as carbonyl groups of CPFX leads to desorption of the drug from the nanocomposite. Under pH 7.4, electrostatic interaction between the drug molecule with PANI/PPy in β-CD is higher due to lower ionization ability (insolubility) of the drug which lowers the release content.

## Conclusion

β-CD/PPy and β-CD/PANI nanocomposites were successfully synthesized via ultrasonication. The intense electrostatic interactions via hydrogen bonding between NH of PPy, PANI and OH of β-CD were confirmed via FTIR studies. UV studies also established the variation in the polaronic transition peak of PPy and PANI which could be interrelated to the formation of β-CD based nanocomposites of PPy and PANI. XRD results revealed the structure of the β-CD/PPy and β-CD/PANI nanocomposites to be semicrystalline. SEM studies revealed encapsulation by PANI/PPy polymeric chains. The synthesized β-CD/PPy and β-CD/PANI nanocomposites were well-suited as ideal drug carriers and could be used to deliver antibiotics in a controlled release manner.

**Supplementary Information** The online version contains supplementary material available at https://doi.org/10.1007/s00289-022-04667-4.

**Acknowledgements** The authors wish to acknowledge National Science Foundation (Award # 2122044), the NSF PREM for Hybrid Nanoscale Systems between NCCU and Penn State, for providing financial assistance.

## References

1. Javanbakht S, Pooresmaeil M, Namazi H (2019) Green one-pot synthesis of carboxymethyl cellulose/Zn-based metal-organic framework/grapheme oxide bio-nanocomposite as a nano-carrier for drug delivery system. Carb Polym 208:294–301
2. Hua Q, Suna W, Wang C, Gua Z (2016) Recent advances of cocktail chemotherapy by combination drug delivery systems. Adv Drug Del Rev 98:19–34
3. Karimzadeh Z, Javanbakht S, Namazi H (2019) Carboxymethyl cellulose/MOF-5/graphene oxide bio-nanocomposite as antibacterial drug nanocarrier agent. BioImpacts 9(1):5–13
4. Jadoun S, Ashraf SM, Riaz U (2019) Insights into the spectral, thermal and morphological effects of co-oligomerization of pyrrole with luminol: a comparative experimental and computational study. Mater Sci Eng B 273:115396
5. Riaz U, Ashraf SM, Verma A (2016) Influence of conducting polymer as filler and matrix on the spectral, morphological and fluorescent properties of sonochemically intercalated poly(o-phenylenediamine /montmorillonite nanocomposites. Recent Pat Nanotech 10(1):66–76
6. Riaz U, Ahmad S, Ashraf SM (2008) Influence of polymerization conditions on the template free synthesis of nanoparticles of poly (1-naphthylamine). Polym Bull 60(4):487–493
7. Riaz U, Ashraf SM, Verma A (2015) Recent advances in the development of conducting polymer intercalated clay nanocomposites: a short review. Curr Org Chem 19(13):1275–1291
8. Mir A, Kumar A, Riaz U (2022) short review on the synthesis and advance applications of polyaniline hydrogels. RSC Adv 12(30):19122–19132
9. Zia J, Ajeer M, Riaz U (2019) Visible–light driven photocatalytic degradation of Bisphenol-a using ultrasonically synthesized polypyrrole/ K-birnessite nanohybrids: experimental and DFT studies. J Environ Sci 79:161–173
10. Ashraf SM, Ahmad S, Riaz U, Dua R (2005) Conducting semi-interpenetrating polymer network of polypyrrole with poly (esteramide urethane) synthesized from a sustainable resource. J Macromol Sci A Pure Appl Chem 42:521–533
11. Zia J, Riaz U (2020) Studies on the spectral, morphological and magnetic properties of PCz-PPy copolymer encapsulated $BaFe_2O_4$ nanohybrids. J Mater Sci Mater Elect 31(24):22856–22865
12. Zia J, Kashyap J, Riaz U (2018) Facile synthesis of polypyrrole encapsulated $V_2O_5$ nanohybrids for visible light driven green sonophotocatalytic degradation of antibiotics. J Mol Liq 272:834–850
13. Verma A, Riaz U (2018) Sonolytically intercalated poly(anisidineco-toluidine)/bentonite nanocomposites: pH responsive drug release characteristics. J Drug Del Sci Tech 48:49–58
14. Verma A, Riaz U (2018) Mechanochemically synthesized poly(o-toluidine)-intercalated montmorillonite nanocomposites as antituberculosis drug carriers. Int J Polym Mater Polym Biomater 67(4):221–228
15. Verma A, Riaz U (2019) Synthesis, characterization and in vitro drug release studies of sonolytically intercalated poly(o-anisidine)/montmorillonite nanocomposites. Macrom Res 27:140–152
16. Khan S, Aazam ES, Jain SK (2020) Synthesis and characterization of β-cyclodextrin/poly(1-naphthylamine) inclusion complex and in-vitro release studies of metformin hydrochloride. J of Polym and the Envir 28:1106–1116
17. Ashraf SM, Ahmad S, Riaz U (2004) Synthesis, characterization and in vitro drug release studies of sonolytically intercalated poly(o-anisidine)/montmorillonite nanocomposites. J Appl Polym Sci 93:82
18. Geetha S, Rao CRK, Vijayan M, Trivedi DC (2006) Biosensing and drug delivery by polypyrrole. Anal Chim Acta 568(1–2):119–125
19. Liu X, Gilmore KJ, Moulton S, Wallace G, Jalili AR, Esrafilzadeh D, Razal JM (2016) A novel and facile approach to fabricate a conductive and biomimetic fibrous platform with sub-micron and micron features. J Mater Chem B 4:1056–1063

20. Olszowy P, Szultka M, Ligor T, Mowaczyk J, Buszewsk B (2010) Fibers with polypyrrole and polythiophene phases for isolation and determination of adrenolytic drugs from human plasma by SPME-HPLC. J Chromatogr B 878:2226–2234
21. Hong S, Li Z, Li C, Dong C, Shuang S (2018) β-cyclodextrin grafted polypyrrole magnetic nanocomposites toward the targeted delivery and controlled release of doxorubicin. Appl Surf Sci 427:1189–1198
22. Shang S, Zeng W, Tao X (2012) Fabrication of conducting polypyrrole/b-cyclodextrin nano- and microspheres using molecular templates. RSC Adv 2:4675–4682
23. Yang YF, Meng FY, Li XH, Wu NN, Deng YH, Wei LY, Zeng XP (2019) Magnetic graphene oxide-$Fe_3O_4$-PANI nanoparticle adsorbed platinum drugs as drug delivery systems for cancer therapy. J Nanosci Nanotechnol 12:7517–7525
24. Chapman CAR, Cuttaz EA, Goding JA, Green RA (2020) Actively controlled local drug delivery using conductive polymer-based devices. Appl Phys Lett 116:010501
25. Shah SAA, Firlak M, Berrow SR, Halcovitch NR, Baldock SJ, Yousafzai BM, Hathout RM, Hardy JG (2018) Electrochemically enhanced drug delivery using polypyrrole films. Materials 11(7):1123
26. Ge D, Qi R, Mu J, Ru X, Hong S, Ji S, Linkov V, Shi W (2010) A self-powered and thermally-responsive drug delivery system based on conducting polymers. Electroche Commu 12:1087–1090
27. Svirskis D, Wright BE, Sejdic JT, Rodgers A, Garg S (2010) Evaluation of physical properties and performance over time of an actuating polypyrrole based drug delivery system. Senso Actua B Chem 151:97–102
28. Alshammary B, Walsh FC, Herrasti P, de Leon CP (2016) Electrodeposited conductive polymers for controlled drug release: polypyrrole. J S State Electrochem 20:839–859
29. Samanta D, Meiser JL, Zare RN (2015) Polypyrrole nanoparticles for tunable, pH-sensitive and sustained drug release. Nanoscale 7:9497–9504
30. Li S, Jasim A, Zhao W, Fu L, Ullah MW, Shi Z, Yang G (2018) Fabrication of pH-electroactive bacterial cellulose/polyaniline hydrogel for the development of a controlled drug release system. ES Mater Manuf 1:41–49
31. Vivek R, Wang LP, Wada S, Wang JY (2018) Nanostructured polyaniline: synthesis and application for photothermal cancer therapy. Curr Appl Polym Sci 2:18–26
32. Basavaiah K, Pavan Kumar Y, Rao AVP (2013) A facile one-pot synthesis of polyaniline/magnetite nanocomposites by micelles-assisted method. Appl Nanosci 3:409–415
33. Verma A, Riaz U (2018) Spectral, thermal and morphological characteristics of ultrasonically synthesized poly(anisidine-cophenylenediamine)/ bentonite nanocomposites: a potential antidiabetic drug carrier. J Mol Liq 261:1–13
34. Seul KY, Seul DS, Jeong DW, Shim JH (2017) Development and application of cyclodextrin hydrolyzing mutant enzyme which hydrolyzes β- and γ-CD selectively. J Agric Food Chem 65(11):2331–2336
35. Pooresmaeil M, Namazi H (2018) Preparation and characterization of polyvinyl alcohol/β-cyclodextrin/ GO-Ag nanocomposite with improved antibacterial and strength properties. Polym Adv Technol 30:447–456
36. Namazi H, Heydari A, Pourfarzolla A (2013) Synthesis of glycoconjugated polymer based on polystyrene and nanoporous β-cyclodextrin to remove copper (II) from water pollution. Int J Polym Mater Polym Biomater 63:1–6
37. Hirayama F, Uekama K (1999) Cyclodextrin-based controlled drug release system. Adv Drug Deliv Rev 36:125–141
38. Chordiya MA, Senthilkumaran K (2012) Cyclodextrin in drug delivery: a review. Res Rev J Pharm Pharma Sci 6:329–357
39. Namazi H, Heydari A (2014) Synthesis of β-cyclodextrinbased dendrimer as a novel encapsulation agent. Polym Int 63(8):1447–1455
40. Chena Y, Song L, Chen Z, Zhang L, Wua W (2015) Morphology and properties of polypyrrole/cyclodextrin nanowires using molecular templates. Desig Monom Polym 18:35–41
41. Storsberg J, Ritter H, Pielartzik H, Groenendaal L (2000) Cyclodextrins in polymer synthesis: supramolecular cyclodextrin complexes of pyrrole and 3,4-ethylenedioxythiophene and their oxidative polymerization. Adv Mater 12:567–569
42. Rokovic MK, Persi B, Mandic Z (2010) Electrochemical synthesis of polyaniline from anilne/cyclodextrin solutions. J Electroanal Chem 643:46–51

43. Feng JT, Yan W, Zhu J (2010) Synthesis of novel hexagonal micro-sheet polypyrrole and micro-sheet polypyrrole with grooves in the presence of α-cyclodextrin/acid red G inclusion compounds. Synth Met 160:939–945
44. Chen W, Wan X, Xu N, Xue G (2003) Ordered conducting polypyrrole doped with sulfopropyl ether of β-cyclodextrin. Macromolecules 36:276–278
45. Lee JY, Park SM (1998) Electrochemistry of guest molecules in thiolated cyclodextrin self-assembled monolayers: an implication for size-selective sensors. J Phys Chem B 102:9940–9945